LUT University

Evaluating and optimizing of steam ejector performance considering heterogeneous condensation using machine learning framework

Momeni Dolatabadi Amir, Mottahedi Hamid Reza, Faghih Aliabadi Mohammad Ali, Saffari Pour Mohsen, Wen Chuang, Akrami Mohammad

This is a Author's accepted manuscript (AAM) version of a publication

published by Elsevier

in Energy

DOI: 10.1016/j.energy.2024.132240

Copyright of the original publication:

© 2024 Elsevier Ltd.

Please cite the publication as follows:

Momeni Dolatabadi, A., Mottahedi, H.R., Faghih Aliabadi, M.A., Saffari Pour, M., Wen, C., Akrami, M. (2024). Evaluating and optimizing of steam ejector performance considering heterogeneous condensation using machine learning framework. Energy, vol. 305. DOI: 10.1016/j.energy.2024.132240

This is a parallel published version of an original publication. This version can differ from the original published article.

Evaluating and optimizing of steam ejector performance considering heterogeneous condensation using Machine learning framework

Amir Momeni Dolatabadi[a], Hamid Reza Mottahedi[b], Mohammad Ali Faghih Aliabadi [1c], Mohsen Saffari Pour[d], Chuang Wen[e,f], Mohammad Akrami[f,]

[a] School of Energy Systems, P.O. Box 20, Lappeenranta-Lahti University of Technology LUT, Lappeenranta 53851, Finland
[b] Department of Mechanical Engineering, Ferdowsi University of Mashhad, Mashhad, Iran
[c]Faculty of Mechanical and Energy Engineering, Shahid Beheshti University, Tehran, Iran
[d] Department of Mechanical Engineering, Faculty of Engineering, Shahid Bahonar University of Kerman, Kerman, Iran
[e] School of the Built Environment, University of Reading, Reading RG6 6AH, United Kingdom
[f] College of Engineering, Mathematics and Physical Sciences, University of Exeter, Exeter EX4 4QF, UK

Abstract

In the context of global warming and pollution concerns, refrigeration systems have become pivotal in energy conversion system. Within this realm, ejector types that harness renewable energy resources emerge as promising alternatives, offering a pathway towards environmentally conscious and resilient energy practices. Under specific conditions, condensation within the heat exchanger results in diverse droplet sizes at the ejector inlet, inducing homogeneous-heterogeneous condensation (HMTC) and heterogeneous condensation (HTC) phenomena. This study aims to evaluate and improve the performance of steam ejectors by investigating and optimizing the effects of homogeneous condensation (HMC), HTC, HMTC, and evaporation processes using a machine learning (ML) framework. The drone squadron optimization (DSO), Particle Swarm Optimization (PSO), and Genetic Algorithm (GA) are chosen and used in the ML framework to find the optimal droplet radius and number. Findings predict that the presence of 10^{18} 1/kg droplets with a radius of 0.02 μm (Optimal mode) at the inlet results in a 2.6% increase in the entrainment ratio (E_r) and a 6.9% reduction in the entropy generation compared to the baseline mode. Generally, the research reveals that HTC exhibits superior performance compared to prevailing theories, leading to enhanced ejector performance.

Keywords: Ejector performance, Non-equilibrium homogeneous condensation, heterogeneous condensation, Entrainment ratio, Optimization, Machine learning.

Nomenclature

CR	Compression Ratio (-)	τ	Viscous Stress Tensor (Pa)
E	Total Energy (J)	σ	Liquid Surface Tension (n/m)
E_r	Entrainment Ratio (-)	Γ	Mass Generation Rate $(kg/m^3.s)$
h	Enthalpy (J/kg)	*Subscripts*	
J	Nucleation Rate $(1/kg.s)$	d	Discharge
Kn	Knudsen Number	hom	Homogeneous
k	Turbulent Kinetic Energy (J/kg)	het	Heterogeneous
K_b	Boltzmann's Constant	i,j,k	Direction
M_c	Convective Mach Number	l	Liquid
m	Molecular Mass (kg)	lv	Liquid-Vapor
$\dot{m}$	Mass Flow Rate (kg/s)	$grow$	Growth
n	Number of Liquid Droplets $(1/kg)$	nuc	Nucleation
P	Pressure (Pa)	p	Primary

[1] Email (*Corresponding authors): faghih.mohamad@yahoo.com , m_faghihaliabadi@sbu.ac.ir

q_c	Condensation Coefficient	s	Secondary
r	Droplet Radius (m)	sat	Saturation
R	Gas Constant $(J/kg.K)$	v	Vapor
T	Temperature (K)	$*$	Critical Condition
t	Time (s)	*Acronyms*	
u, v	Velocity Components (m/s)	ANN	Artificial Neural Network
x	Cartesian Direction (m)	CFD	Computational Fluid Dynamics
y	Liquid Mass Fraction (-)	DSO	Drone Squadron Optimization
Greek symbols		ERS	Ejector Refrigeration System
γ	Heat Capacity Ratio	GA	Genetic Algorithm
ω	Specific Dissipation Rate $(1/s)$	HMC	Homogeneous Condensation
ρ	Density (kg/m^3)	$HMTC$	Homogeneous-heterogeneous Condensation
μ	Dynamic Viscosity $(Pa.s)$	HTC	Heterogeneous Condensation
λ	Thermal Conductivity $(W/m.K)$	LMF	Liquid Mass Fraction
		PSO	Particle Swarm Optimization

1. Introduction

The increasing awareness of the importance of thermal comfort, driven by climate changes and rising temperatures, has emphasized the significance of the refrigeration and air conditioning industry. However, conventional refrigeration cycles are known to contribute significantly to energy consumption and greenhouse gas emissions [1-2]. The use of environmentally harmful working fluids in conventional refrigeration cycles has raised concerns regarding their impact on the environment. Consequently, there is a growing importance in adopting refrigeration cycles that operate with environmentally friendly working fluids. Ejector refrigeration system (ERS) can be a suitable alternative for conventional refrigeration cycles [3]. ERSs utilize low-grade waste energy from industrial processes, solar energy, and geothermal energy, thereby reducing fossil energy consumption and greenhouse gas emissions [4]. By harnessing these alternative energy sources, ERSs contribute to a more sustainable approach in refrigeration, offering potential benefits for both energy efficiency and environmental conservation. Also, ERS has the ability to use water vapor working fluid. Fig. 1 illustrates the schematic of the ERS within a solar-driven system.

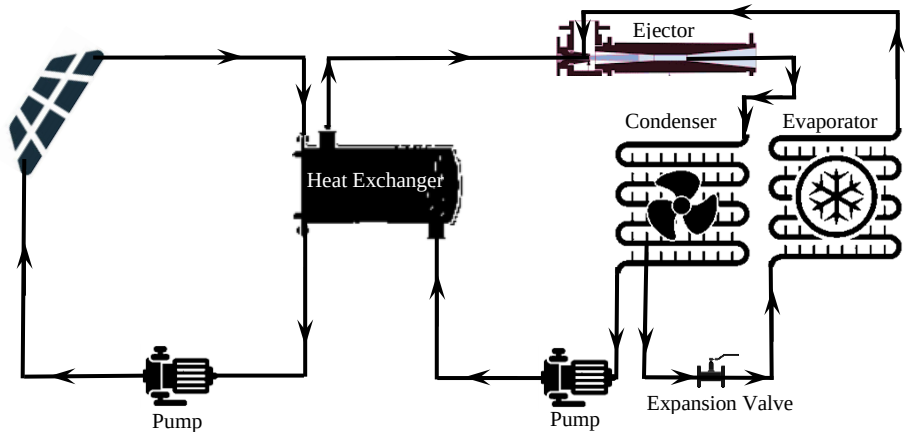

Fig.1. The solar-driven ERS.

The ejector system, one of the notable components in a refrigeration system, has garnered significant attention in recent years due to its reliance on thermally triggered energy [5-6]. A pivotal element within these cycles is the ejector, playing a fundamental role in initiating the system. Comprising four essential components—namely, the primary nozzle, suction chamber, mixing part, and diffuser (as depicted in Fig. 2)—the supersonic ejector operates on the principle of accelerating the primary flow or driver output from the generator. This acceleration occurs within a converging and diverging nozzle until the flow reaches an ultrasonic state. As the secondary flow gains momentum and encounters acoustic conditions within the mixing shear layer, it forms a mixed flow that further expands. This expansion leads to shock occurrences within the fixed cross-section throat, causing the flow to transition from supersonic to subsonic states before passing through the diffuser and reaching the ejector outlet at the condenser inlet [7-8].

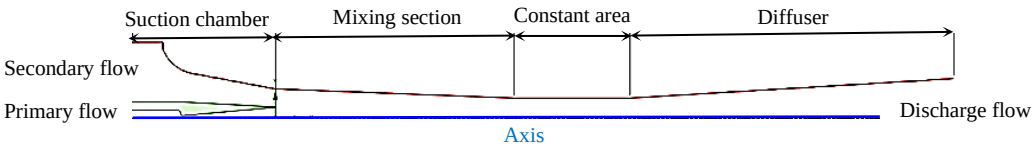

Fig.2. A typical steam ejector configuration [8].

The losses incurred within ejectors present a significant challenge, making any endeavor to mitigate these losses highly valuable. Chen et al. [9] conducted an exhaustive evaluation of the ejector refrigeration cycle using advanced exergy analysis. Their meticulous calculations of advanced exergy destruction within cycle components revealed that over 50% of the total exergy destruction occurs in the ejector. They concluded that enhancing ejector performance could notably improve cycle efficiency. Similarly, Haghparast et al. [10] highlighted the potential for enhancing ejector cooling cycles by deeply understanding ejector features. Through numerical and experimental investigations, they emphasized the crucial role of

identifying key ejector dimensions. Their findings underscored that minimizing exergy losses holds the key to optimizing ejector performance for enhanced efficiency.

The exploration of ejector efficiency through Computational Fluid Dynamics (CFD) has been extensive in recent studies. Galindo et al. [11] scrutinized the impact of various refrigerants—R1234yf, R1234ze, and R600a—on solar ejector refrigeration cycle efficiency. They emphasized the role of optimizing ejector geometry in restoring cycle performance and leveraged CFD to compute suction ratios for different ejector configurations and operational conditions, with R1234yf exhibiting superior performance. Similarly, Banasiak et al. [12] conducted numerical analyses, highlighting the significant influence of mixer mass flow on ejector efficiency using R744 refrigerant. Their investigation into mixer diameter and length underscored their pronounced impact on entropy generation. Sierra-Pallares et al. [13] focused on entropy generation analysis in ejectors with R134a refrigerant, pinpointing local entropy production to identify irreversibility's within the ejector and linking reductions to geometrical alterations, with over 75% of entropy production attributed to viscous dissipation. Fu et al. [14] delved into primary nozzle geometry variations' effect on ejector performance, establishing an optimal range for primary nozzle outlet diameter and emphasizing the negligible role of diverging part length on performance. Ruangtrakoon et al. [15] explored shock location in mixing flows and primary jet expansion angle's impact on ejector performance. Wang et al. [16] improved ejector performance by modifying primary nozzle geometry and surface roughness, emphasizing the significance of throat and divergent part design due to their sensitivity to geometric dimensions. Dong et al. [17] underscored the substantial influence of mixing chamber structure on ejector efficiency, especially regarding different mixing chamber lengths' effects on suction ratio and critical back pressure. Besagni et al. [18] emphasized the critical role of ejectors in refrigeration cycle efficiency, highlighting the impact of fluid dynamics on ejector system enhancement. They advocated for the $k-\omega\,SST$ turbulence model for accurate flow prediction in diverse ejector geometries. Mazzelli et al. [19] compared turbulence models in air ejector simulations, finding the $k-\omega\,SST$ model to yield more accurate predictions, particularly in entrainment rate estimation, across both two-dimensional and three-dimensional simulations.

Refrigeration systems' reliance on ozone-depleting refrigerants poses a significant environmental concern, prompting exploration into environmentally friendly alternatives like water. However, steam-based ejector cycles face challenges, notably lower coefficient of

performance and entrainment ratio (E_r). Researchers and engineers are thus focused on improving system performance, particularly delving into the condensation flow regime within ejectors. Tang et al. [20] conducted experiments revealing abundant droplets in the supersonic jet flow, showcasing a varied droplet size distribution. Wang et al. [21] highlighted the oversight of homogeneous condensation (HMC) in many studies, employing the wet steam model to examine the impact of surface roughness and area ratio. Their findings showcased substantial latent heat release during condensation, impacting pressure and Mach number. Zhang et al. [22] utilized a surface tension model to enhance ejector performance by optimizing the primary nozzle, harnessing a new modeling approach for condensing flow regime simulation. Ariafar et al. [23] observed that in the wet steam model, the ratio of suction to critical back pressure surpasses that of the ideal gas model by 10% to 7%, emphasizing the wet steam model's differences and implications in system behavior.

In recent times, researchers have been focusing on the investigation of heterogeneous condensation (HTC) in various industrial equipment [24-26]. Zhang et al. [27] successfully reduced condensation within the nozzle by introducing salt particles at a specific concentration. Their findings demonstrated that the injection of salt particles had both enhancing and inhibiting effects on the condensation process. Eghbali et al. [28] proposed a strategic approach to minimize the mass fraction of the liquid phase in the flow, aiming to mitigate the negative consequences of condensation shock. Their research indicated a notable decrease in homogeneous nucleation by increasing the number of droplets injected through the nozzles.

There have been numerous studies applying various optimization methods to acquire efficient energy [29-30]. For instance, Ahmed and Chen [31] developed an artificial neural network (ANN) model of a steam ejector and analyzed how different training strategies affect the ANN model's ability to make accurate predictions. Three optimizing algorithms (ADAM, Ftrl, and Adadelt) were applied for ANN model training, with the maximum deviation of their findings from the experimental values being less than 2.5%. Similarly, Cao et al. [32] evaluated and proposed two novel biogas-based cogeneration systems. The optimal mode of their findings showed that the thermal efficiency and the exergy efficiency of the system were maximized up to 57.11% and 36.68%, respectively. Sangesaraki et al. [33] proposed a novel geothermal-based system for hydrogen liquefaction. They applied a ML optimization method

to reduce the calculation time. Among the subsystems, the double flash cycle had the highest exergy destruction rate.

In this study, a steam ejector of refrigeration cycle is simulated, focusing on the condensing flow regime and efficient energy modeling of the vapor-liquid two-phase flow. The liquid phase is initiated through the phenomenon of nucleation, and vapor supercooling leads to non-equilibrium condensation, fostering the growth of liquid droplets. Shock trains, oblique shocks, and continuous expansion-compression processes in the ejector induce condensation-evaporation processes, significantly shaping the two-phase flow pattern. Under specific conditions, homogeneous nucleation and condensation within the heat exchanger result in diverse droplet sizes at the ejector inlet, inducing HMC, HTC, and homogeneous-heterogeneous condensation (HMTC). Moreover, the presence of liquid droplets at the ejector inlet emerges as a crucial factor influencing the condensing flow regime, with injection parameters (droplet size, number, and liquid mass fraction (LMF)) playing a key role in performance. The objectives of this study are outlined as follows:

- Investigating the impact of HTC and HMTC on the non-equilibrium condensing flow regime.
- Conducting and creating a roadmap of steam ejector performance under the presence and absence of phenomena (HMC, HTC, and HMTC) to enhance and access efficient energy.
- Integrating Drone Squadron Optimization (DSO), Particle Swarm Optimization (PSO), and Genetic Algorithm (GA) into the ML framework. Indeed, local optimization can lead to suboptimal solutions during the optimization process. To tackle this issue, a ML framework combines three algorithms (DSO, PSO, GA) to escape local optimal and identify the real optimal mode.
- Applying the ML framework as an optimizer to predict the optimal size of droplets and enhance ejector performance.

2. Methodology

In this section, method solution, equations, and validation have discussed in more detail.

2.1.Method solution

In the current study, the behavior of steam in non-equilibrium condensing conditions through a steam ejector has been simulated using an axisymmetric model. To solve the governing equations, Ansys Fluent is applied as the solver. The governing equations involved momentum, mass, and energy conservation equations. This set of equations is presented as [34-35]:

$$\frac{\partial \rho}{\partial t} + \frac{\partial (\rho u_j)}{\partial x_j} = 0 \quad (1)$$

$$\frac{\partial (\rho u_i)}{\partial t} + \frac{\partial (\rho u_j u_i + P\delta_{ji})}{\partial x_j} - \frac{\partial \tau_{ji}}{\partial x_j} = 0 \quad (2)$$

$$\frac{\partial (\rho E)}{\partial t} + \frac{\partial (\rho u_j H)}{\partial x_j} + \frac{\partial (q_j - u\tau_{ji})}{\partial x_j} = 0 \quad (3)$$

Likewise, the liquid-phase equations (nucleation and growth equations) have been added [36] to calculate liquid-phase characteristics (Sections 2.2.1-2.2.2). The presence of droplets has led to increased turbulence in the flow. Additionally, the $SST\ k-\omega$ turbulence model is applied [37]. For simulating the viscous condensing steam flow, the $k-\omega\ SST$ model is selected due to its efficiency in modeling both near and far-wall regions. This model, developed by Menter [38], has the following equations:

$$\frac{\partial (\rho k)}{\partial t} + \frac{\partial (\rho k u_j)}{\partial x_j} = \frac{\partial}{\partial x_j}\left((\mu + \frac{\mu_t}{\sigma_k})\frac{\partial k}{\partial x_j}\right) + G_k - Y_k + S_k \quad (4)$$

$$\frac{\partial (\rho \omega)}{\partial t} + \frac{\partial (\rho \omega u_j)}{\partial x_j} = \frac{\partial}{\partial x_j}\left((\mu + \frac{\mu_t}{\sigma_\omega})\frac{\partial \omega}{\partial x_j}\right) + \frac{\alpha}{v_t} G_k - Y_\omega + D_\omega + S_\omega \quad (5)$$

Numerical simulation has been established as a highly reliable tool for modeling fluid flow within ejectors. It enables an accurate representation of various flow phenomena occurring within the flow regime, including mixing, shock waves, boundary layers, compressibility, phase change, supersonic flow, and complex flows. The governing equations are solved by numerical simulation based on the finite volume method. Transport, nucleation, and growth equations were discretized using a density-based, implicit second-order upwind scheme. Convective terms were discretized using the Roe flux-difference scheme [39-40]. To ensure convergence, residuals were plotted against iterations, with convergence criteria set at values below $10^{-6.}$ Finally, an ML framework has been applied as an optimizer to predict the optimal size of droplets and enhance the E_r.

2.2.Liquid-phase modeling

HMC [41] and HTC [42] theories elucidate distinct mechanisms governing phase change phenomena in vapor systems. HMC involves the transition of vapor molecules into liquid droplets without the presence of foreign particles, occurring when the vapor becomes supersaturated [43]. In contrast, HTC occurs when vapor molecules condense onto foreign particles or surfaces, such as dust, aerosols, or existing liquid droplets. The latter provides sites for condensation, facilitating the phase transition even at lower saturation levels. While

HMC manifests within a clean vapor environment, HTC occurs in the presence of nucleation sites, catalyzing the phase change process [44]. Understanding these theories is crucial in various applications, particularly in refining heat transfer processes, designing efficient refrigeration systems, and comprehending atmospheric phenomena. In this study, foreign particles and cores are droplets that have nucleated in the heat exchanger. Fig. 3 shows the structure of HMC and HTC in the condensing steam flow.

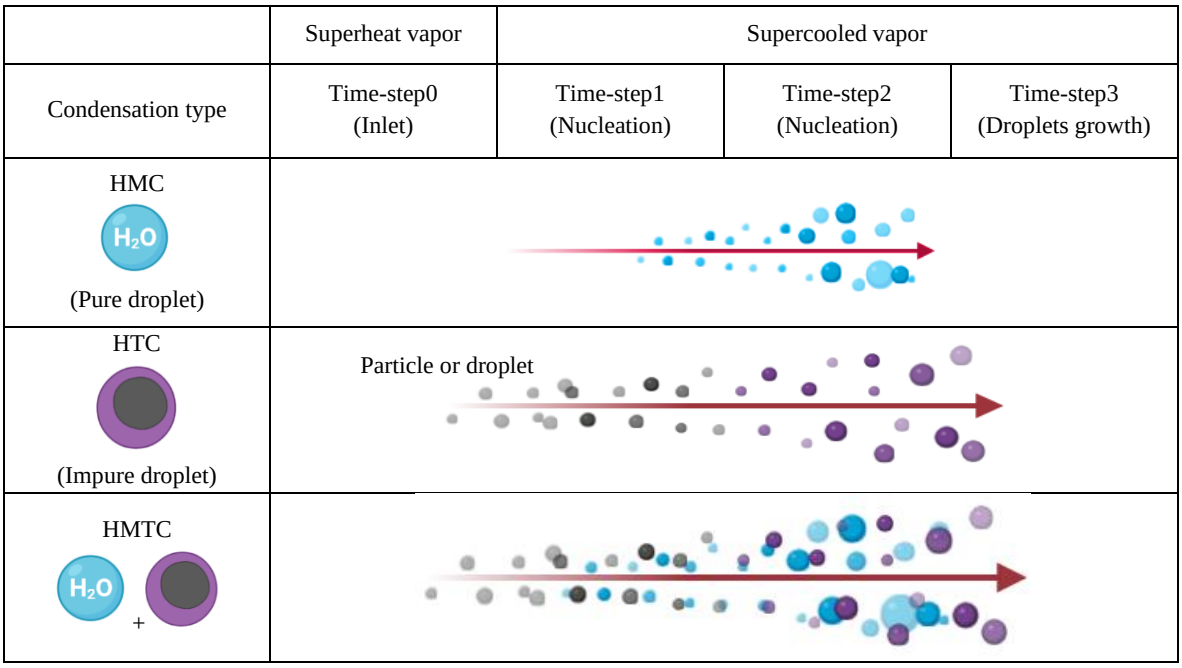

Fig.3. The schematic of the HMC, HTC, HMTC phenomena.

For modeling HMC and HTC, the equations of liquid droplets are individually solved for the droplets at the ejector entrance (HTC) and the droplets nucleated from the HMC phenomena occurring through the primary nozzle of the refrigeration system. On the other hand, the droplet growth equation is the same for both HMC and HTC phenomena. Therefore, the droplet growth equation referenced from [45-46] has been utilized:

$$\frac{dr}{dt} = \frac{\lambda_v (r - r^*)(T_{sat} - T_v)}{\rho_l r^2 (1 + 3.18Kn)(h_v - h_l)} \quad (6)$$

$$T_l = T_{sat}(P) - (T_{sat}(P) - T_v)\frac{r^*}{r} \quad (7)$$

2.2.1. HMC

In this research, a model of monodispersed is utilized to model HMC. Within the nucleation zone of each control volume, numerous droplets are generated, and their quantity in each control volume is determined using Eq. (8) [47]:

$$\frac{\partial(\rho n_{hom})}{\partial t}+\frac{\partial(\rho u_j n_{hom})}{\partial x_j}=\rho J \tag{8}$$

In the context of HMC, $\Gamma_{nuc,hom}$ signifies the droplet mass created due to nucleation, while $\Gamma_{grow,hom}$ represents the droplet mass condensed as a result of droplet growth [48]:

$$\Gamma_{nuc,hom}=\frac{4}{3}\pi\rho_l\rho r^{*3}J \tag{9}$$

$$\Gamma_{grow,hom}=4\pi\rho_{l,hom}\rho n_{hom}r_{het}^2\frac{dr}{dt}_{hom} \tag{10}$$

$$\frac{\partial(\rho y_{hom})}{\partial t}+\frac{\partial(\rho u_j y_{hom})}{\partial x_j}=\Gamma_{nuc,hom}+\Gamma_{grow,hom} \tag{11}$$

$$r_{hom}=(\frac{3y_{hom}}{4\pi\rho_{l,hom}n_{hom}})^{1/3} \tag{12}$$

$$J_{class}=q_c\sqrt{\frac{2\sigma_r}{\pi}}m^{-3/2}\frac{\rho_v}{\rho_l}exp\,(\frac{-4\pi r^{*2}\sigma_r}{3K_bT_v}) \tag{13}$$

The symbol q_c represents the condensation coefficient, typically considered as 1 [49], while K_b denotes the Boltzmann constant, and m signifies the mass of a molecule. Following this, various corrections, such as the Kantrowitz corrections, were incorporated into the classical nucleation equation, as seen in Eq. (14) [50-51]:

$$J=\frac{1}{1+\emptyset}J_{class} \tag{14}$$

$$\emptyset=2\frac{(\gamma-1)}{(\gamma+1)}\frac{h_{lv}}{RT_v}\left(\frac{h_{lv}}{RT_v}-\frac{1}{2}\right) \tag{15}$$

$$r^*=\frac{2\sigma_r}{\rho_l RT_v ln\,(\frac{P}{P_{sat}(T_v)})} \tag{16}$$

2.2.2. HTC

The external particles like NaCl or water droplets can act as nuclei in HTC. This study specifically employs water droplets as external cores for HTC. As the steam deviates from equilibrium, the droplets of liquid injected at the nozzle inlet initiate growth. The equations governing the evolution of these injected droplets at the nozzle inlet are solved for their behavior [52-53]:

$$\frac{\partial(\rho y_{het})}{\partial t}+\frac{\partial(\rho u_j y_{het})}{\partial x_j}=\Gamma_{grow,het} \tag{17}$$

$$\frac{\partial(\rho n_{het})}{\partial t}+\frac{\partial(\rho u_j n_{het})}{\partial x_j}=0 \tag{18}$$

$$\Gamma_{grow,het} = 4\pi\rho_{l,het}\rho n_{het} r_{het}^2 \frac{dr}{dt}_{het} \quad (19)$$

$$r_{het} = \left(\frac{3y_{het}}{4\pi\rho_{l,het} n_{het}}\right)^{1/3} \quad (20)$$

2.2.3. Entropy generation

Similar to conventional energy analysis, the utilization of entropy analysis based on the second law of thermodynamics is a crucial tool for evaluating the performance of energy systems. Entropy generation is defined as follows [54]:

$$S_{gen} = \left(\dot{m}_p + \dot{m}_s\right)s_d - \dot{m}_p s_p - \dot{m}_s s_s \quad (21)$$

3. Validations and Calculations

This section is divided into two segments. The first focuses on the calculations and validations of non-equilibrium condensing flow, detailing the intricacies of the condensation process within the system. The second part centers on validating the behavior of the flow through the ejector system. This bifurcation allows for a comprehensive examination of both the fundamental aspects of non-equilibrium condensing flow and the performance of the ejector.

3.1.Non-equilibrium condensing flow

The nozzles establish a condensation flow regime, resulting in a two-phase flow due to the nucleation phenomenon induced by non-equilibrium conditions. To validate this, the Moore's nozzle B configuration [55] is employed. Similarly, Table 1 presents the boundary conditions. Mesh size plays a crucial role in numerical simulations, directly influencing the accuracy and reliability of results. Optimal mesh sizing ensures the proper resolution of flow features and prevents numerical artifacts, thereby enhancing the computational model's fidelity. Grid independence is confirmed (Table 2) with 59,520 computational cells identified for validation purposes (Fig. 4). Accurate predictions of wall-bounded flows in computational fluid dynamics simulations rely on the proper determination of y^+ values. Hence, Fig. 5 displays the distribution of y^+ values for Moore's nozzle B, which are around 1. Finally, based on the results depicted, agreeable pressure distribution results, with an error of less than 5% from experimental data, have been achieved (Fig. 5).

Table 1

The boundary conditions through nozzle [55].

Nozzles#	Inlet				Outlet
	Type	Pressure	Temperature	Intensity	Pressure
Moore's nozzle B	Pressure-inlet	25 kPa	358 K	1%	5 kPa

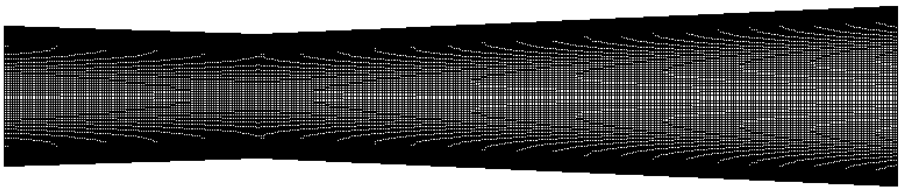

Moore's nozzle B (120×496)

Fig.4. The schematic of mesh of nozzles that applied to validate.

Table 2
The list of grid independence under average of the LMF at outlet of Moore's nozzle B.

Mesh#	Mesh size 1 120×197	Mesh size 2 120×246	Mesh size 3 120×307	Mesh size 4 120×496	Mesh size 5 120×461
LMF at outlet of Moore's nozzle	0.03987	0.04007	0.04128	0.04564	0.004565

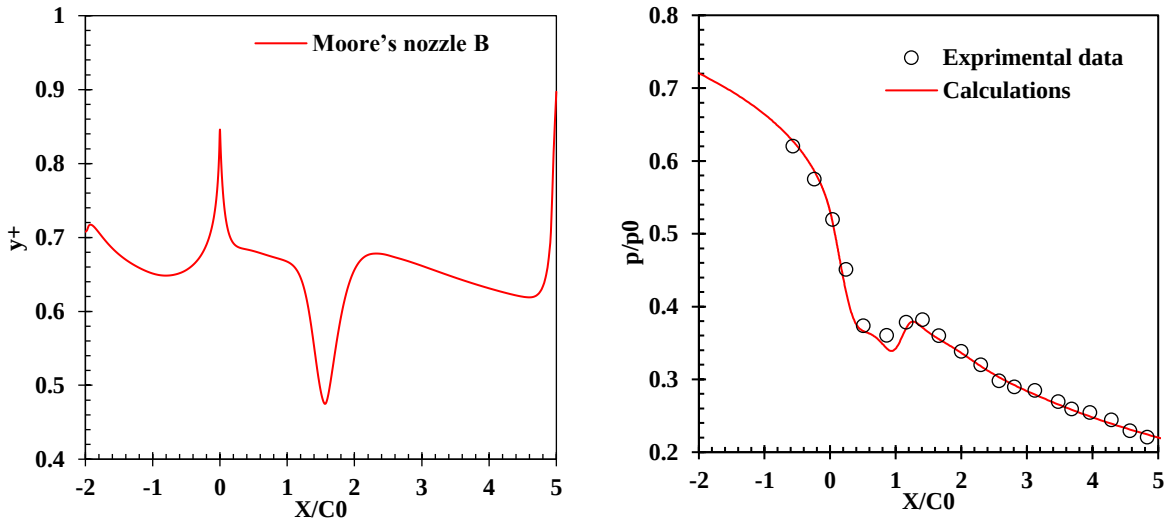

a) y+ **b) Validation**

Fig.5. The distribution of pressure and y+ a long the Moore's nozzle B.

3.2.ejector's performance

The primary parameters crucial for a steam ejector encompass compression and E_r, which are mathematically expressed by the following equations [56-57]:

$$ER = \frac{\dot{m}_s}{\dot{m}_p} \tag{21}$$

$$CR = \frac{P_d}{P_s} \tag{22}$$

The secondary mass flow rate ($\dot{m}_s$) and primary mass flow rate ($\dot{m}_p$), as illustrated in Fig. 6, are significant in the context of the ejector's function. Additionally, P_d and P_s denote the back pressure and the pressure of secondary flow, respectively. The ejector operation categorizes into three distinct conditions outlined in Fig. 6: single-choked, dual-choked, and reverse flow. In the dual-choked flow condition, both nozzles experience choking due to the pressure of discharge being lower than the pressure of critical, maintaining a constant E_r. As the pressure of discharge rises, the mode of single-choking occurs, causing a sudden reduction in the secondary stream's mass flow, subsequently decreasing the ratio of entrainment through ejector while the zone of constant area remains unchoked. When the discharge pressure surpasses the pressure of restricting, the ratio of entrainment falls to zero, accompanied by backflow into the secondary flow. Notably, the ejector's performance parameters, such as the compression and E_r, are assessed considering to the equilibrium operating conditions, specifically the mode of dual-choked [58]. To validate these conditions, two ejectors were utilized.

- Ruangtrakoon ejector
- Aldoori ejector

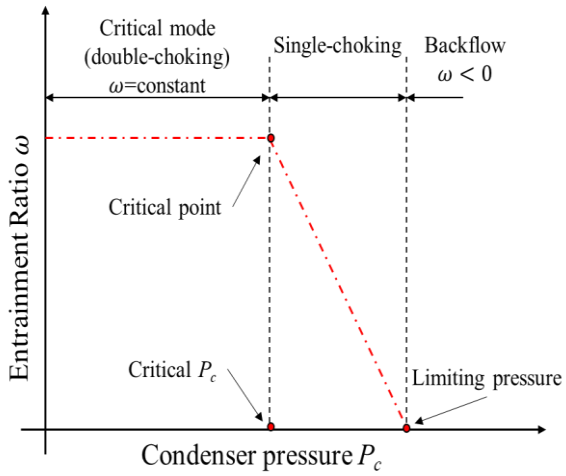

Fig.6. A schematic performance curve of the ejector in which three different modes were depicted [3].

3.2.1. Ruangtrakoon ejector

In this section, validation of the numerical solution is performed against experimental investigation by Ruangtrakoon and Thongtip [59] through the ejector, specifically designed for a renewable refrigeration cycle utilizing water as the working fluid. The comparison in Table 3 details E_r values obtained through numerical simulations against available experimental data. Both primary and secondary flows remain in their saturation states throughout the validation process. The primary flow operates at pressures of 270, 361, and

476 kPa, while the secondary flow maintains a pressure of 1037 Pa. E_r is computed for various nozzle types and inlet flow pressures, and error values are calculated concerning the experimental data. The observed error ranges from 3.5% as the lowest to 5.5% as the highest, signifying a close agreement between the calculated methodology and the observed steam flow behavior within the ejector.

Table 3
Validation summary details with the Ruangtrakoon ejector [58]

Primary nozzle	P_p (kPa)	T_p (℃)	P_s (kPa)	T_s (℃)	P_d (kPa)	ER_{exp} (-)	ER_{Num} (-)	Error (%)
D1.7 M4	270	130	1.037	7.5	3	0.43	0.45	4.6
D1.7 M4	361	140	1.037	7.5	4	0.29	0.30	3.4
D1.7 M4	476	150	1.037	7.5	5	0.18	0.19	5.5
D1.4 M3	476	150	1.037	7.5	3	0.28	0.29	3.5
D2.0 M4	270	130	1.037	7.5	3	0.28	0.29	3.5

3.2.2. Aldoori ejector

In the context of evaluating a steam ejector of refrigeration system under HMTC phenomenon, the Aldoori ejector [60] serves as the key apparatus for simulation. This ejector is specifically engineered to emulate a refrigeration system. Table 4 presents the geometrical attributes of the Aldoori ejector, detailing parameters such as the diameter of the primary nozzle (3.2 mm) and the diameter of the fixed cross-section in the ejector (25.4 mm). Table 5 provides an overview of the boundary conditions applied within the Aldoori ejector setup.

Table 4
Geometric details of the steam ejector

Geometric parameters	Size (mm)
Primary nozzle inlet diameter	10
Primary nozzle throat diameter	3.2
Primary nozzle outlet diameter	13.6
Primary nozzle divergent length	59.5
Mixing chamber inlet diameter	37
Mixing chamber length	155
Constant area zone diameter	25.4
Constant area zone length	75
Subsonic diffuser length	210
Subsonic diffuser outlet diameter	50

Table 5
The boundary condition of steam ejector has used.

Parameters	Conditions			
	Temperature (K)	Pressure (kPa)	Turbulent parameters	
			Turbulence intensity (%)	Turbulent viscosity ratio (-)
Primary	403	270	5	1
Secondary	287	1.6		
Discharge	-	4.2		

In an effort to assess solution sensitivity concerning grid density, a structured quadrilateral cell-based computational grid is constructed. The impact of varying grid densities on the E_r is analyzed, as depicted in Table 6. Additionally, Fig. 7 illustrates the optimized computational domain within the Aldoori ejector. Through a validation summary displayed in Table 6, a comparison between the experimental data and numerical solution is presented. The observed maximum deviation of 6.9% falls within an acceptable error range, affirming the accuracy of the present numerical solution in portraying steam flow characteristics within the ejector.

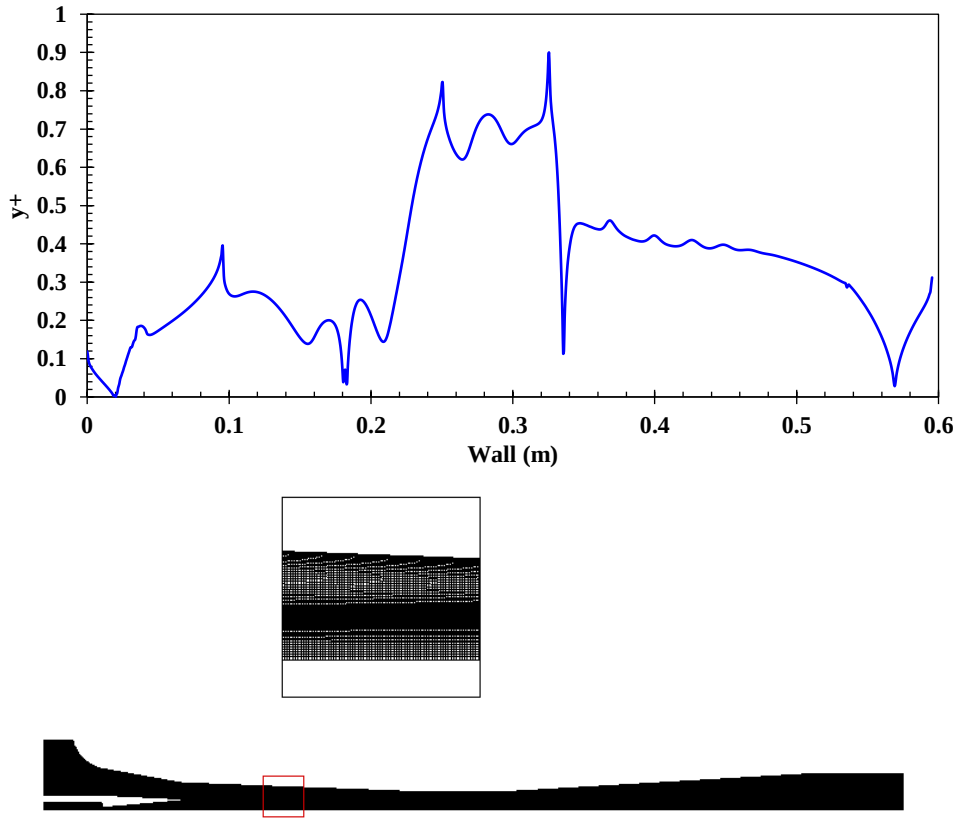

Fig. 7. Optimized mesh size on computational domain and distribution of y^+ have considered ejector (Mesh size 4 :101520 cells).

Table 6
Computational sensitivity grid size and validation summary details of E_r through the Aldoori ejector.

Mesh size (#size)	E_r (-)	
	Experiment results [60]	Calculation results (present study)
Mesh size 1 (11071 cells)	0.33	0.3180
Mesh size 2 (23052 cells)		0.3300
Mesh size 3 (52788 cells)		0.3465
Mesh size 4 (101520 cells)		0.3520
Mesh size 5 (214756 cells)		0.3530
Mesh size 6 (348567 cells)		0.3535

4. Results and discussion

The steam ejector plays a pivotal role in refrigeration systems cycles, yet its limited E_r hampers its widespread use. Efforts to enhance its performance are thus highly regarded. Non-equilibrium condensation is a phenomenon prevalent in steam ejectors, leading to the formation of an HMC flow regime within. This transformation significantly disrupts ejector operation, disturbing the location and intensity of oblique shocks due to the substantial latent heat release. Moreover, under specific conditions, the entrance of the ejector experiences humidity, inducing two phenomena: HTC and HMTC. Currently, the presence of liquid droplets emerges as a key technique in modulating condensation behavior, notably reducing the intensity of oblique shocks. The influence of water droplets is observed across two primary aspects: the number and radius of droplets. At a consistent count of droplets, an augmented inlet humidity correlates with larger injected droplet radii. Conversely, holding the LMF constant, the radius of present droplets decreases as the count of droplets increases. This study aims to evaluate the impact of HMC, HTC, and HMTC phenomena on steam ejector performance. To explore these phenomena, droplets with radii of 0 nm, 13.9 nm, and 64.5 nm were employed to represent HMTC, HTC, and HMC, respectively. The specified inlet LMF for the liquid droplet presence is set at 0.01.

4.1.Behavior of flow analysis

This section investigates the influence of HMC, HTC, and HMTC on Mach number and temperature distribution, presented in Fig. 8 and Fig. 9. In absence of an external core (HMC), steam entering the primary nozzle experiences a drop in temperature at its converging section, resulting in an increase in Mach number, eventually reaching unity at the nozzle throat. As steam continues into the divergent part, temperatures decrease while Mach numbers rise. This continuous expansion prompts spontaneous nucleation, generating tiny

water droplets essential for steam condensation. The presence of these droplets facilitates surface creation for condensation, releasing latent heat into the flow and leading to condensation shock.

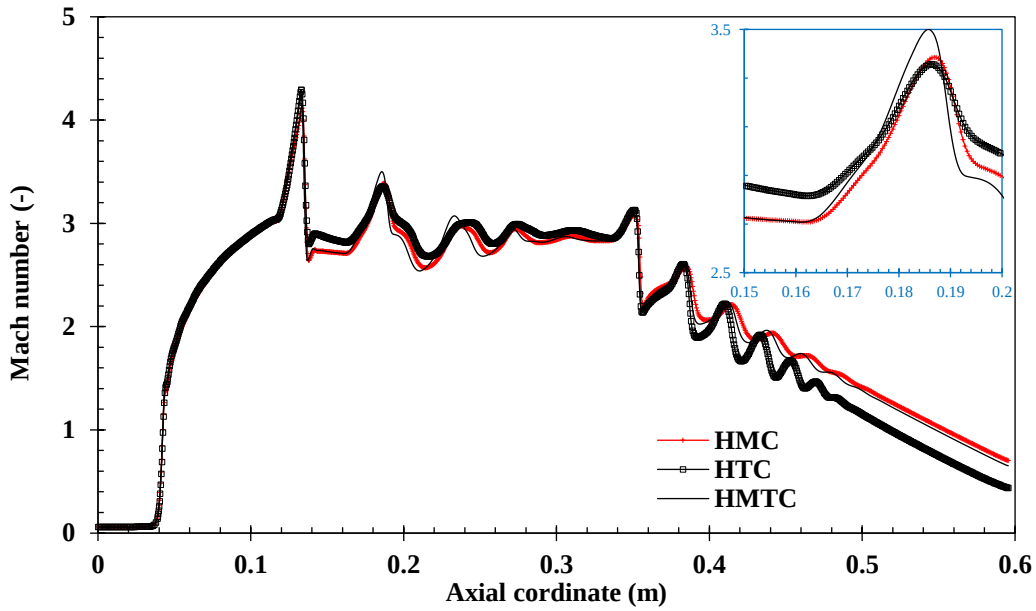

Fig.8. The effects of HMC, HTC, and HMTC phenomena on distribution of Mach number in steam ejector.

Zoomed views in Fig. 8 and Fig. 9 reveal these shocks under HMC, HTC, and HMTC scenarios. HTC and HMTC notably impact the location of condensation shocks. Post-nozzle exit, Mach number and temperature fluctuations occur in the throat, mixing chamber, and diffuser due to expansion waves and oblique shocks. HTC and HMTC also influence these expansion shocks and fluctuations across the nozzle. Fig. 8 and Fig. 9 highlight the considerable effects of HTC and HMTC on temperature distribution and Mach number variations. Notably, HTC demonstrates a pronounced difference compared to other condensation modes. Beyond x>0.38 m, a rapid temperature increase, and significant Mach number reduction are observed compared to other modes. Steam behavior in HMC closely resembles that of HMTC.

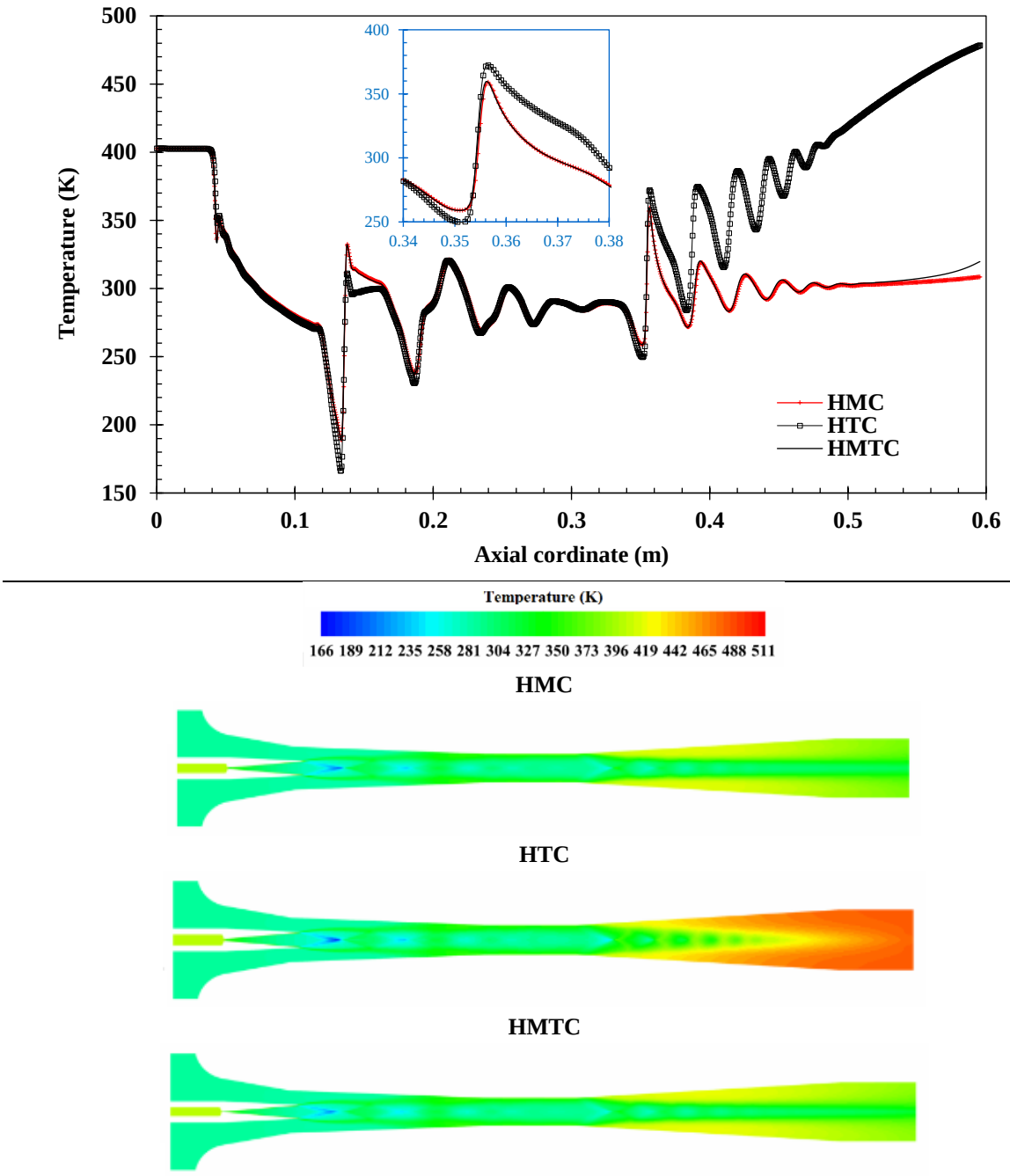

Fig.9. The effects of HMC, HTC, and HMTC phenomena on distribution of temperature through steam ejector.

Non-equilibrium condensation is a fascinating occurrence involving the transformation of vapor into liquid, releasing latent heat that significantly impacts flow patterns. This section scrutinizes the effects of HMC, HTC, and HTC in greater detail to explore their influence on homogeneous and heterogeneous nucleation as well as the supersaturation ratio. Homogeneous nucleation furnishes the necessary surface for steam condensation, resulting in the formation of numerous minuscule water droplets. Fig. 10 demonstrates how HMC, HTC, and HMTC affect nucleation, or the supersaturation ratio. Notably, HTC displays no

significant occurrences, whereas HMTC exhibits a lower nucleation rate than HMC. Fig. 10 illustrates the supersaturation ratio, which reflects the non-equilibrium flow or deviation from the equilibrium state. In thermodynamic equilibrium, this ratio equals one, whereas the phenomenon of nucleation necessitates a high supersaturation ratio to manifest, elucidating why nucleation is less favorable in HTC scenarios.

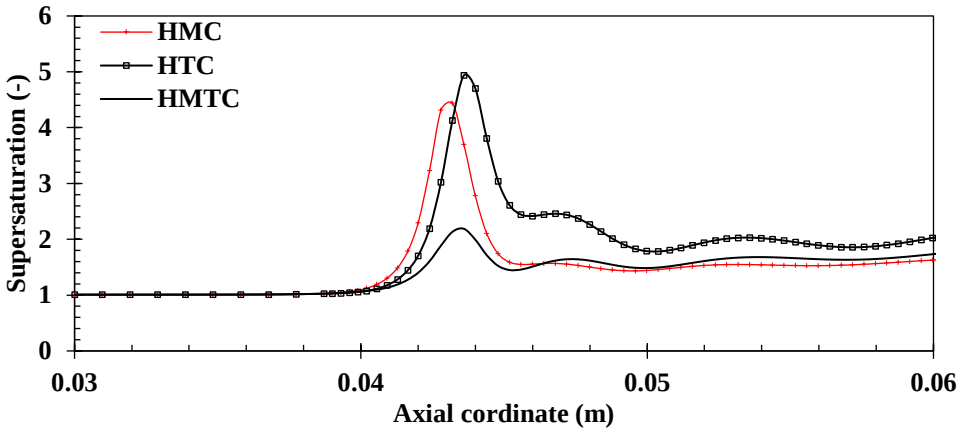

Fig.10. The effects of HMC, HTC, and HMTC phenomena on distribution of supersaturation in steam ejector.

The LMF serves as an indicator reflecting the condensation-evaporation processes within the steam ejector refrigeration setup. When the LMF increases, condensation takes place, while a decrease indicates evaporation tendencies. Fig. 11 and 12 illustrate the impact of HMC, HTC, and HNTC on the homogeneous and heterogeneous distribution of the LMF. At HTC and $x > 0.38$ m, the LMF within the ejector drops to zero, shifting the flow into a single-phase state. The presence of oblique shocks and expansion waves prompts droplets with smaller radii to shift phases more rapidly, transitioning into vapor. Homogeneous distribution of the LMF decreases due to the water droplets presence at the ejector inlet (HTC and HNTC). In HTC scenarios, the homogeneous distribution of the LMF becomes zero as droplets grow, leading to an increase in heterogeneous distribution. Conversely, in HMTC scenarios, the heterogeneous distribution of the LMF decreases, indicating that the radius of injected droplets plays a significant role in influencing homogeneous and heterogeneous distribution of droplet growth or LMF. The most prominent homogeneous distribution of LMF corresponds to the HMC behavior.

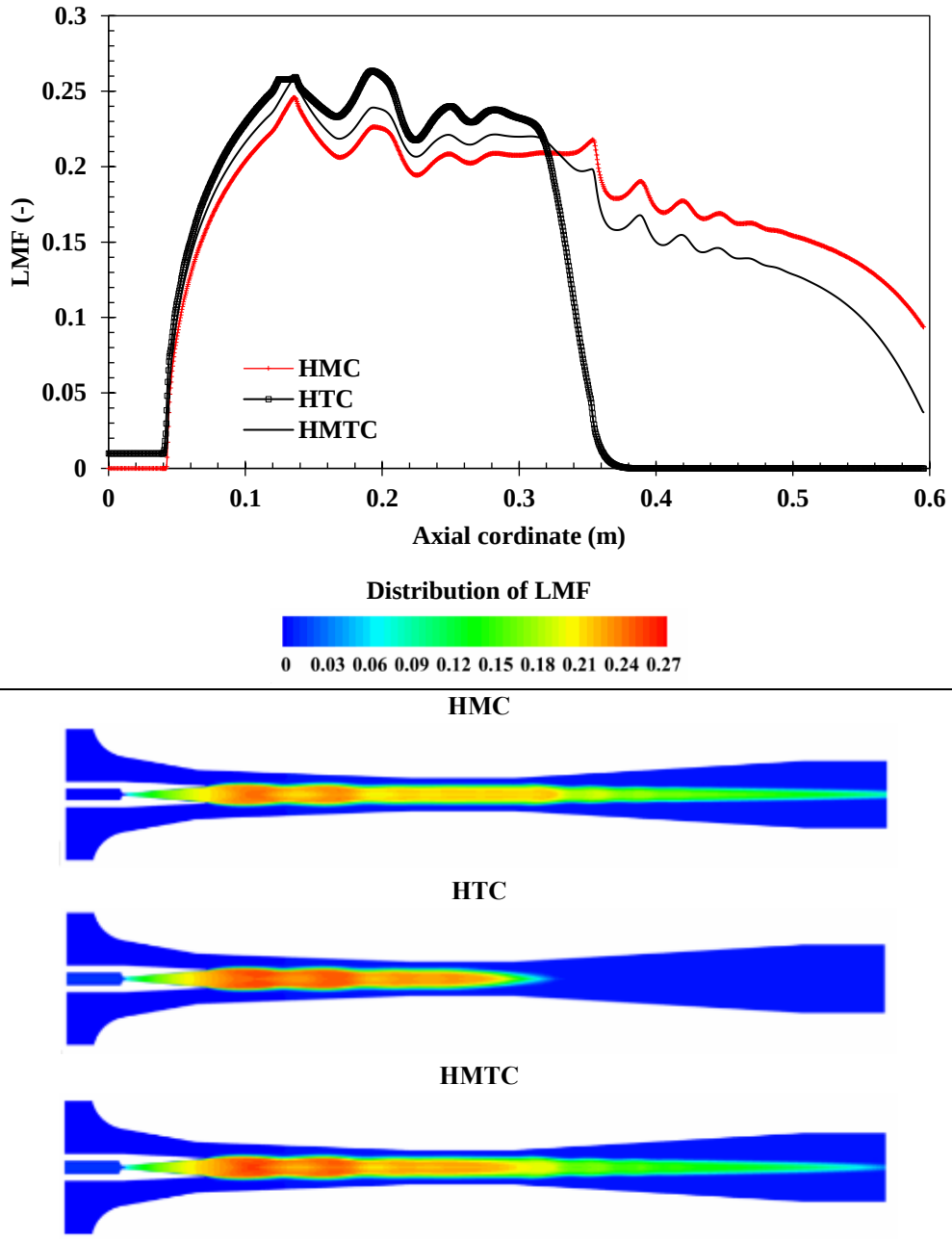

Fig.11. The effects of HMC, HTC, and HMTC phenomena on distribution of LMF through steam ejector.

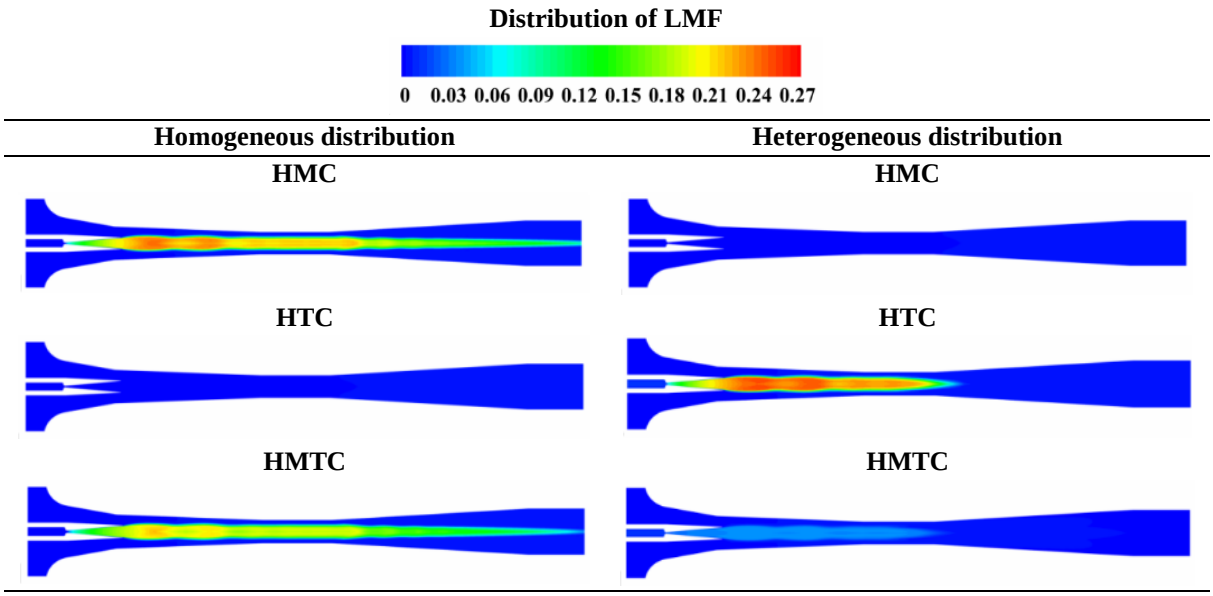

Fig.12. The effects of HMC, HTC, and HMTC phenomena on homogeneous and heterogeneous distribution of LMF through steam ejector.

4.2.Performance analysis

The E_r stands as a pivotal parameter in ejector design, directly impacting its performance. This section scrutinizes the impact of HMC, HTC, and HMTC on the E_r. Fig. 13 shows E_r/E_{r0} under various LMF and droplets number where, E_{r0} is considered as 0.352 for in the absence of droplets. Table 7 provides insights into droplet characteristics like number and radius. Notably, when the droplet count is 10^{18} 1/kg and 10^{19} 1/kg, the condensation type is HTC, displaying a nucleation rate of zero. Meanwhile, at 10^{16} 1/kg and 10^{17} 1/kg droplet counts, the condensation type is a blend of HMTC. Within the 10^{16} 1/kg droplet count, an increase in the LMF (i.e., a rise in droplet radius) doesn't seem to affect the E_r. However, at 10^{17} 1/kg droplets, the E_r decreases with an augmented wetness factor. Interestingly, with 10^{18} 1/kg and 10^{19} 1/kg droplets, the E_r elevates alongside increased LMF. The most substantial rise in the E_r occurs at a 5% concentration of water liquid droplets with a count of 10^{19} 1/kg and a droplet radius of 11 nm, showing a 5.73% increase. This suggests that HTC significantly amplifies the E_r, while in scenarios involving mixed condensation regimes, the ejector's performance either diminishes or remains unchanged.

The impact of HMC, HTC, and HMTC on the primary mass flow rate and secondary mass flow rate can be observed in Figure 14. The m_{p0} and m_{s0} are obtained as 12.01 and 4.237 kg/h for in the absence of droplets. The presence of primary droplets at the inlet of the primary nozzle leads to variations in condensation intensity within the primary nozzle. As depicted in Figure 11, the condensation intensity is higher in HTC compared to HMTC and

HMC. The release of latent heat resulting from condensation affects the primary mass flow rate, causing a reduction in its magnitude. Reference [34] provides a comprehensive explanation of the influence of condensation on the mass flow rate in the nozzle. The decrease in the mass flow rate of the primary flow is more pronounced in HTC than in HMTC. Among different LMFs, 10^{19} 1/kg exhibits the lowest primary flow mass flow rate. In terms of the mass flow rate of the secondary flow, the HTC has the most significant impact, resulting in the highest mass flow rate across different LMFs. Conversely, 10^{19} 1/kg, the secondary mass flow rate reaches its highest value.

Table 7

Condensation types and the maximum nucleation rate for the injected water droplets.

Droplet radius (nm)	**Droplet number** $1/kg$	**LMF (%)**	**Log10 (max droplets nucleation rate)** $1/kg.s$	**Condensation type (-)**
0	0	0	24.57	HMC
64.5	1e+16	1	24.44	HTMC
81.2	1e+16	2	24.35	HTMC
93.0	1e+16	3	24.26	HTMC
102.0	1e+16	4	24.17	HTMC
111.0	1e+16	5	24.13	HTMC
30.0	1e+17	1	23.53	HTMC
37.7	1e+17	2	22.24	HTMC
43.2	1e+17	3	21.84	HTMC
48.6	1e+17	4	21.38	HTMC
53.3	1e+17	5	20.61	HTMC
13.9	1e+18	1	0	HTC
17.5	1e+18	2	0	HTC
20.1	1e+18	3	0	HTC
22.1	1e+18	4	0	HTC
23.8	1e+18	5	0	HTC
6.4	1e+19	1	0	HTC
8.1	1e+19	2	0	HTC
9.3	1e+19	3	0	HTC
10.3	1e+19	4	0	HTC
11.0	1e+19	5	0	HTC

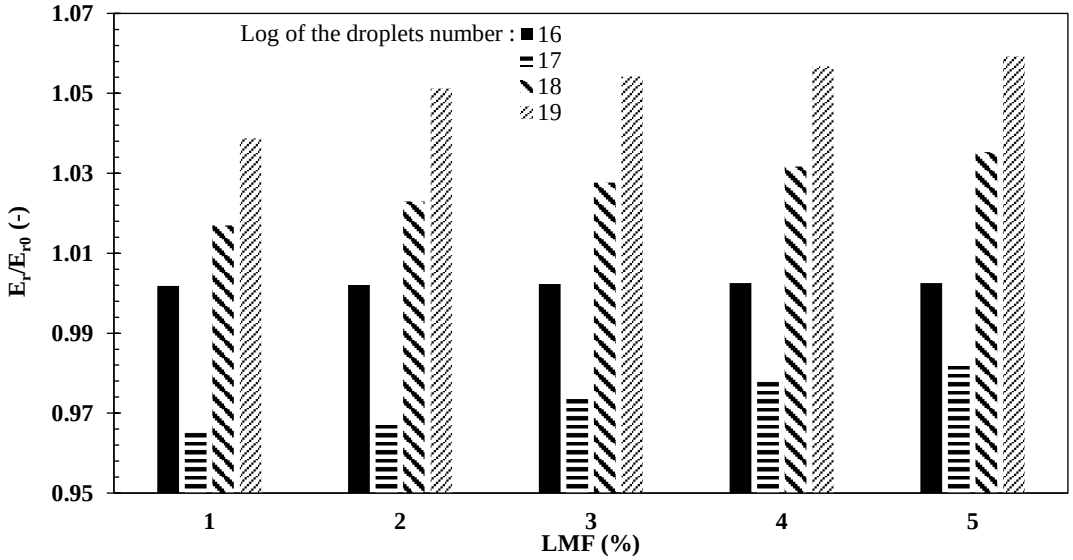

Fig.13. The effects of HMC, HTC, and HMTC phenomena on the E_r of steam ejector.

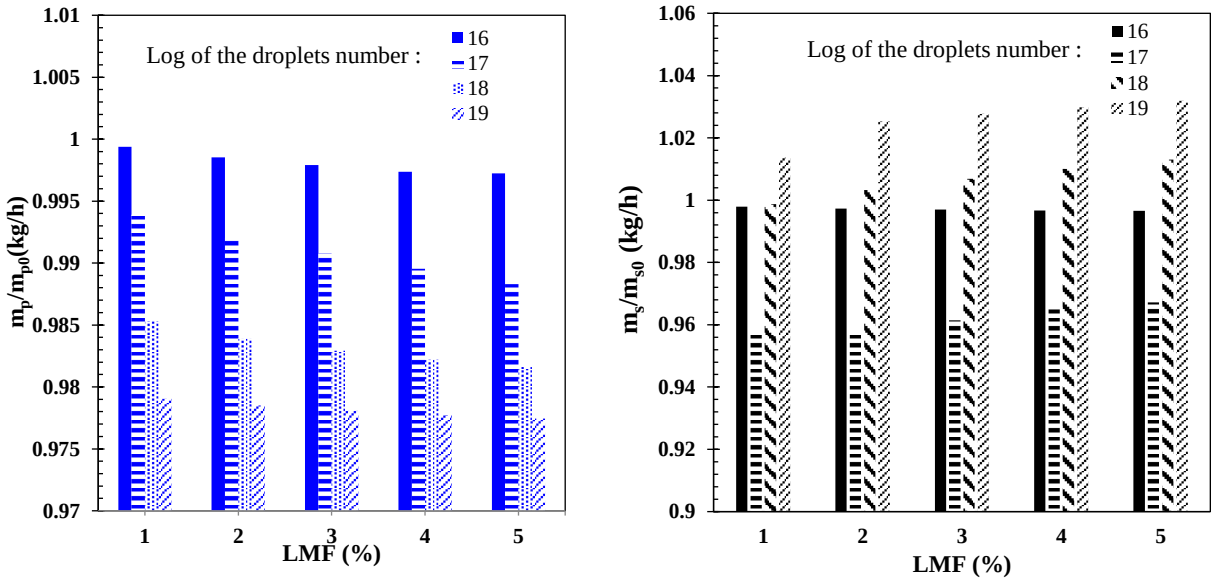

Fig.14. The effects of HMC, HTC, and HMTC phenomena on primary and secondary mass flow rates of the steam ejector.

4.3.ML

The prons and cons of the numerical optimizations are numerous and such diversity would be helpful for researchers to find and predict their optimal models. Tejada-Arango [61], Marini and Walczak [62], and Solomon et al. [63] have presented and discussed the power of optimized prediction of the DSO, PSO, and GA models, respectively. One of the concerns during the optimization is its locality, which refers to finding an optimal location that cope better than other vicinity points around, but not necessarily the global optimal point [64]. To

illustrate this concept, Fig.15 provides an example of the local optimal point and a real optimal point. Therefore, in the present research similar approach have been adopted by three optimization algorithms (DSO, PSO and GA) and combined them using the ML framework to escape from the local optimization and find the real optimal mode.

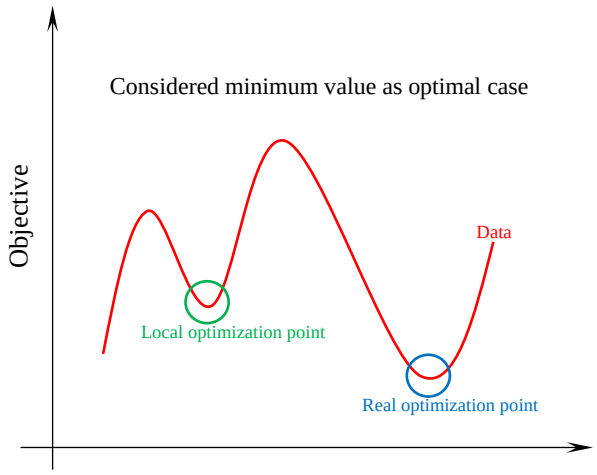

Fig.15. A graphical example of local and real optimization point

The research analysis utilizes a regression framework to create models predicting output characteristics from input attributes. E_r , primary mass flow rate, entropy generation and value of the LMF at the end of the primary nozzles are considered as multi-objective in optimization process. E_r is considered as an indicator of ejector performance, primary mass flow rate is applied as an indicator of consumption energy, entropy generation is employed as an indicator of loss and irremediability parameter and LMF is considered to avoid of loss, erosion, and liquid-film on walls. By integrating the Support Vector Regression (SVR) method [65] into the ML structure, data regression enhancement becomes feasible. The primary goal of support vector machines is to find an optimal hyperplane that minimizes the gap between two classes. The Φ kernel function spreads complex data widely for accurate identification, enabling the linear separation of higher-dimensional data. If provided with a single training dataset residing in D-dimensional space, it's possible to establish a function linking input to output using D characteristics [66]. In the initial stage of the experiment, regression fusion is employed to the training data. a schematic of the learning framework is provided (As shown in Fig. 16,). Initially, random values for ε and C are assigned to each regression classifier. These two variables span a range from 0 to 20. The DSO algorithm [67] leverages the parameters ε and C to identify the configuration that yields the lowest mean

square error (MSE). This process enables a more efficient and precise determination of the effective method. Five repetitions are executed to assess the regression fusion of the pool structure, average accuracy, and best matching parameters. Concerning the matching parameters, the optimal solution is a grid with the highest accuracy rate.

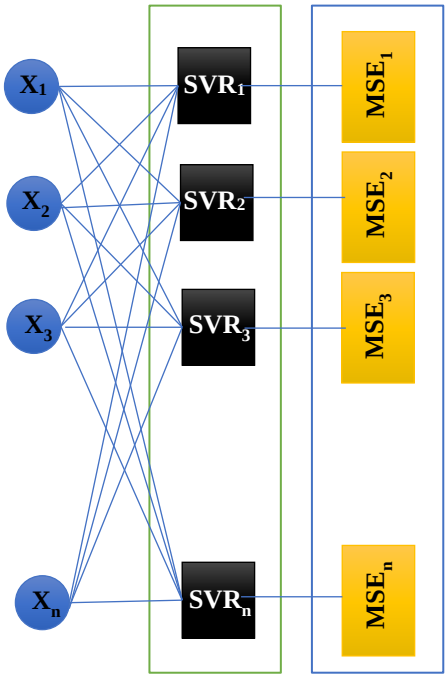

Fig. 16. The regression fusion scheme relies on a pool of Support Vector Regression (SVR) models.

Heuristic algorithms often encounter two main challenges: becoming trapped in local optimal points and experiencing premature convergence. A meta-heuristic algorithm is a type of approximate optimization algorithm designed to address these issues and can be applied across a wide range of scenarios. When drones operate over the same terrain, they may produce nearly identical target coordinates, potentially leading to local optima. However, drones can potentially avoid these local optima by employing convergence avoidance techniques, which are not typically found in most evolutionary algorithms. Significant disparities were observed between the DSO algorithm and its alternatives across various metrics. These differences can be attributed to DSO's convergence avoidance mechanism, which utilizes techniques such as mat Interval, Opposition, and scaling's to promote exploration [68-69]. Stagnation control mechanisms prevent the hill-climbing approach by allowing for the consideration of suboptimal solutions. According to Fig. 17, the parameters of the DSO algorithm outperform those of GA and PSO algorithms in escaping local optima, a common challenge in optimization. This observation is supported by a comprehensive

examination of a large dataset. The optimal mode of droplet number and size is presented and compared with the mode without droplets, listed in Table 8.

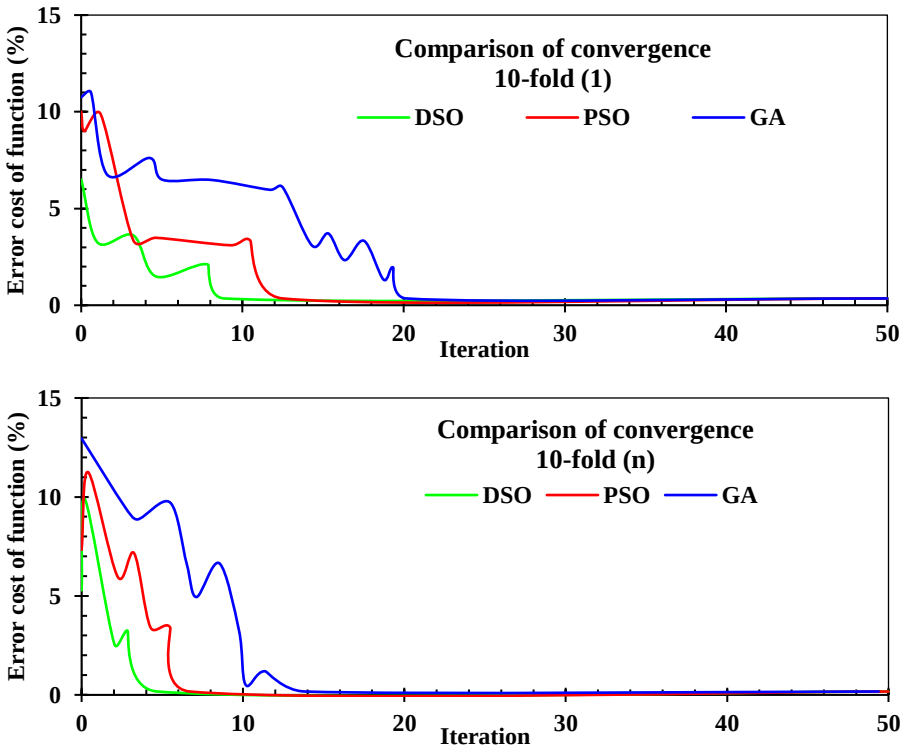

Fig. 17. The convergence and speed of the DSO approach are compared to various optimization procedures for improving the SVR learning performance in the pool of fusion model.

Table8
Compare optimal mode with original mode of steam ejector.

Modes	Characters			Entropy generation (W/K)	E_r	$LMF_{at\ NXP}$	$\dot{m}_p$ (kg/h)
	$n_{at\ inlet}$ (1/kg)	$r_{at\ inlet}$ (μm)	$LMF_{at\ inlet}$				
Original mode	0	0	0	5.74	0.352	0.21	12.01
Optimal mode	10^{18}	0.02	~3%	5.33	0.361	0.24	11.70

5. Conclusion

The steam ERS is of significant importance due to its potential to offer efficient and environmentally friendly cooling solutions, thereby advancing both technology and sustainability in refrigeration. One of the most impactful factors affecting the efficiency of this system is the condensation-evaporation process. In this research, a comprehensive assessment of a steam ejector under the HMC, HTC, and HMTC phenomena has been conducted. This evaluation begins with the validation of simulated results against existing experimental data for a steam ejector. Furthermore, the influence of various condensation

types on two-phase flow behavior was investigated. Finally, three optimization algorithms—DSO, PSO, and GA—were integrated into a machine learning framework as optimizers to predict the optimal type of condensation and enhance the performance of ejector. The following concluding remarks could be listed as:

- Liquid droplet injection parameters have a definite effect on the type of condensation. The incidence of HTC alone leads to an increase in the performance of the ejector, and the simultaneous existence of HTC and HMC primes to a decrease/negligible effect on the performance. The highest intensification in the $E_r$is observed at 5% concentration. For instance, presence of droplets at inlet of ejector with the number of 10^{19} 1/kg and the radius of 11nm, the increase in the E_r is 5.73%.
- The presence of 10^{18} 1/kg droplets with a radius of 0.02 μm at the inlet was chosen as the optimal mode. The optimal droplet configuration resulted in a 2.6% increase in the E_r and a 7.1% reduction in entropy generation compared to the baseline mode.

In summary, steam ERS, favored for their environmental compatibility and low emissions, have drawn global attention despite their inherent low efficiency. As a potential avenue for future research, it is recommended to pursue further optimization and exploration of novel geometries under HTC to enhance the performance of steam ejectors.

Declaration of generative AI and AI-assisted technologies in the writing process

During the preparation of this work the authors used ChatGPT 3.5 in order to improve language and readability. After using this tool/service, the authors reviewed and edited the content as needed and take full responsibility for the content of the publication.

References

[1] Mota-Babiloni A, Barbosa Jr JR, Makhnatch P, Lozano JA. Assessment of the utilization of equivalent warming impact metrics in refrigeration, air conditioning and heat pump systems. Renewable and Sustainable Energy Reviews. 2020 Sep 1;129:109929.

[2] Sun Z, Li J, Liang Y, Sun H, Liu S, Yang L, Wang C, Dai B. Performance assessment of CO2 supermarket refrigeration system in different climate zones of China. Energy conversion and management. 2020 Mar 15;208:112572.

[3] Zhang G, Dykas S, Li P, Li H, Wang J. Accurate condensing steam flow modeling in the ejector of the solar-driven refrigeration system. Energy. 2020 Dec 1;212:118690.

[4] Liu B, Guo X, Xi X, Sun J, Zhang B, Yang Z. Thermodynamic analyses of ejector refrigeration cycle with zeotropic mixture. Energy. 2023 Jan 15;263:125989.

[5] Huang Y, Jiang P, Zhu Y. Experimental and modeling studies of thermally-driven subcritical and transcritical ejector refrigeration systems. Energy conversion and management. 2020 Nov 15;224:113361.

[6] Shen A, Guan K, Yang X, Jin S, Yang L. Theoretical analysis of a novel liquid-vapor separation condensation ejector refrigeration cycle with zeotropic mixtures. Energy conversion and management. 2020 Nov 1;223:113322.
[7] Jahangiri A, Aliabadi MA, Pourranjbar D, Mottahedi HR, Gharebaei H, Ghamati E. A comprehensive investigation of non-condensable gas and condenser temperature effects on power plant ejector performance by considering condensation flow regime. Thermal Science and Engineering Progress. 2023 Sep 16:102128.
[8] Aliabadi MA, Bahiraei M. Effect of water nano-droplet injection on steam ejector performance based on non-equilibrium spontaneous condensation: A droplet number study. Applied Thermal Engineering. 2021 Feb 5;184:116236.
[9] Chen J, Havtun H, Palm B. Conventional and advanced exergy analysis of an ejector refrigeration system. Applied Energy. 2015 Apr 15;144:139-51.
[10] Haghparast P, Sorin MV, Nesreddine H. The impact of internal ejector working characteristics and geometry on the performance of a refrigeration cycle. Energy. 2018 Nov 1;162:728-43.
[11] Galindo J, Dolz V, García-Cuevas LM, Ponce-Mora A. Numerical evaluation of a solar-assisted jet-ejector refrigeration system: Screening of environmentally friendly refrigerants. Energy Conversion and Management. 2020 Apr 15;210:112681.
[12] Banasiak K, Palacz M, Hafner A, Buliński Z, Smołka J, Nowak AJ, Fic A. A CFD-based investigation of the energy performance of two-phase R744 ejectors to recover the expansion work in refrigeration systems: An irreversibility analysis. International journal of refrigeration. 2014 Apr 1;40:328-37.
[13] Sierra-Pallares J, Del Valle JG, Carrascal PG, Ruiz FC. A computational study about the types of entropy generation in three different R134a ejector mixing chambers. International Journal of Refrigeration. 2016 Mar 1;63:199-213.
[14] Fu W, Li Y, Liu Z, Wu H, Wu T. Numerical study for the influences of primary nozzle on steam ejector performance. Applied Thermal Engineering. 2016 Aug 5;106:1148-56.
[15] Ruangtrakoon N, Thongtip T, Aphornratana S, Sriveerakul T. CFD simulation on the effect of primary nozzle geometries for a steam ejector in refrigeration cycle. International Journal of Thermal Sciences. 2013 Jan 1;63:133-45.
[16] Wang L, Yan J, Wang C, Li X. Numerical study on optimization of ejector primary nozzle geometries. International Journal of Refrigeration. 2017 Apr 1;76:219-29.
[17] Dong J, Hu Q, Yu M, Han Z, Cui W, Liang D, Ma H, Pan X. Numerical investigation on the influence of mixing chamber length on steam ejector performance. Applied Thermal Engineering. 2020 Jun 25;174:115204.
[18] Besagni G, Inzoli F. Computational fluid-dynamics modeling of supersonic ejectors: Screening of turbulence modeling approaches. Applied Thermal Engineering. 2017 May 5;117:122-44.
[19] Mazzelli F, Little AB, Garimella S, Bartosiewicz Y. Computational and experimental analysis of supersonic air ejector: Turbulence modeling and assessment of 3D effects. International Journal of Heat and Fluid Flow. 2015 Dec 1;56:305-16.
[20] Tang Y, Liu Z, Li Y, Yang N, Wan Y, Chua KJ. A double-choking theory as an explanation of the evolution laws of ejector performance with various operational and geometrical parameters. Energy Conversion and Management. 2020 Feb 15;206:112499.
[21] Wang C, Wang L, Zou T, Zhang H. Influences of area ratio and surface roughness on homogeneous condensation in ejector primary nozzle. Energy Conversion and Management. 2017 Oct 1;149:168-74.
[22] Zhang G, Zhang X, Wang D, Jin Z, Qin X. Performance evaluation and operation optimization of the steam ejector based on modified model. Applied Thermal Engineering. 2019 Dec 25;163:114388.

[23] Ariafar K, Buttsworth D, Al-Doori G, Malpress R. Effect of mixing on the performance of wet steam ejectors. Energy. 2015 Dec 15;93:2030-41.
[24] Zhang G, Yang Y, Chen J, Jin Z, Dykas S. Numerical study of heterogeneous condensation in the de Laval nozzle to guide the compressor performance optimization in a compressed air energy storage system. Applied Energy. 2024 Feb 15;356:122361.
[25] Hu P, Liang Q, Fan T, Wang Y, Li Q. Investigation of heterogeneous condensation flow characteristics in the steam turbine based on homogeneous-heterogeneous condensation coupling model using OpenFOAM. Energy. 2024 Mar 29:131108.
[26] Kortsensteyn NM, Levashov VY, Yastrebov AK, Petrov LV. Numerical simulation of homogeneous-heterogeneous condensation and interphase heat transfer in a dusty vapour-gas flow: Controlling the homogeneous condensation process. International Journal of Thermal Sciences. 2024 Jun 1;200:108966.
[27] Zhang G, Wang X, Chen J, Tang S, Smołka K, Majkut M, Jin Z, Dykas S. Supersonic nozzle performance prediction considering the homogeneous-heterogeneous coupling spontaneous non-equilibrium condensation. Energy. 2023 Dec 1;284:129274.
[28] Eghbali MJ, Tavakol M, Khoei ET, Tamimi M, Amini R. Enhancing steam flow efficiency through fine droplet injection in nozzles: Mitigating wetness losses and condensation shock. Applied Thermal Engineering. 2024 Feb 8:122657.
[29] Dolatabadi AM, Pour MS, Rezaee K, Ajarostaghi SS. Applying machine learning for optimization of dehumidification strategy on the modified model for the non-equilibrium condensation in steam turbines. Engineering Analysis with Boundary Elements. 2022 Dec 1;145:13-24.
[30] Megdouli K, Tashtoush B, Cinnella P. Application of machine learning to enhance the performance of a two-stage, two-temperature ejector cycle driven by the waste heat of exhaust gas. Energy Conversion and Management. 2024 Feb 15;302:118091.
[31] Ahmed F, Chen W. Investigation of steam ejector parameters under three optimization algorithm using ANN. Applied Thermal Engineering. 2023 May 5;225:120205.
[32] Cao Y, Dhahad HA, Hussen HM, Parikhani T. Proposal and evaluation of two innovative combined gas turbine and ejector refrigeration cycles fueled by biogas: Thermodynamic and optimization analysis. Renewable Energy. 2022 Jan 1;181:749-64.
[33] Sangesaraki AG, Gharehghani A, Mehrenjani JR. 4E analysis and machine learning optimization of a geothermal-based system integrated with ejector refrigeration cycle for efficient hydrogen production and liquefaction. International Journal of Hydrogen Energy. 2023 Sep 30;48(82):31875-904.
[34] Aliabadi MA, Jahangiri A, Khazaee I, Lakzian E. Investigating the effect of water nano-droplets injection into the convergent-divergent nozzle inlet on the wet steam flow using entropy generation analysis. International Journal of Thermal Sciences. 2020;149:106181.
[35] Dolatabadi AM, Eghbali MJ, Florin-Emilian Ț, Mohamadpour E, Amini R. Performance evaluation of condensing flow behavior considering magneto hydrodynamics field effects. Applied Thermal Engineering. 2023 Jan 25;219:119472.
[36] Hosseini SA, Nakisa M, Lakzian E. Reducing the condensing flow effects on the steam turbine blades through modified design geometry. Physics of Fluids. 2023 Sep 1;35(9).
[37] Nikiforow K, Koski P, Karimäki H, Ihonen J, Alopaeus V. Designing a hydrogen gas ejector for 5 kW stationary PEMFC system–CFD-modeling and experimental validation. International Journal of Hydrogen Energy. 2016 Sep 7;41(33):14952-70.
[38] Menter FR, Kuntz M, Langtry R. Ten years of industrial experience with the SST turbulence model. Turbulence, heat and mass transfer. 2003;4(1):625-32.

[39] Abadi SN, Ahmadpour A, Abadi SM, Meyer JP. CFD-based shape optimization of steam turbine blade cascade in transonic two phase flows. Applied Thermal Engineering. 2017;112:1575-89.
[40] Dykas S, Wróblewski W. Single-and two-fluid models for steam condensing flow modeling. International Journal of Multiphase Flow. 2011;37(9):1245-53.
[41] Aliabadi MA, Lakzian E, Khazaei I, Jahangiri A. A comprehensive investigation of finding the best location for hot steam injection into the wet steam turbine blade cascade. Energy. 2020;190:116397.
[42] Ding H, Zhang Y, Yang Y, Wen C. A modified Euler-Lagrange-Euler approach for modelling homogeneous and heterogeneous condensing droplets and films in supersonic flows. International Journal of Heat and Mass Transfer. 2023 Jan 1;200:123537.
[43] Hosseinizadeh SE, Ghamati E, Jahangiri A, Majidi S, Khazaee I, Aliabadi MA. Reduction of water droplets effects in steam turbine blade using Multi-objective optimization of hot steam injection. International Journal of Thermal Sciences. 2023 May 1;187:108155.
[44] Sun W, Pen J, Niu L, Jiang Z, Hu W, Pan LM. Sensitivity analysis of nucleation and droplet growth models in the prediction of natural gas non-equilibrium condensation in Laval nozzle. Applied Thermal Engineering. 2024 Jan 5;236:121562.
[45] zhang Wang H. Energy and exergy analysis of primary steam superheating effects on the steam ejector applied in the solar renewable refrigeration cycle in the presence of spontaneous nucleation. Chemical Product and Process Modeling. 2024 Feb 22;19(1):51-68.
[46] Aliabadi MA, Lakzian E, Jahangiri A, Khazaei I. Numerical investigation of effects polydispersed droplets on the erosion rate and condensation loss in the wet steam flow in the turbine blade cascade. Applied Thermal Engineering. 2020;164:114478.
[47] Dolatabadi AM, Salmani F, Lakzian E. Analysis of heterogeneous nucleation and erosion behavior considering the injection of impurities into wet steam flow using poly-dispersed method. International Journal of Heat and Mass Transfer. 2022 Apr 1;185:122392.
[48] Zhang G, Wang X, Dykas S, Aliabadi MA. Reduction entropy generation and condensation by NaCl particle injection in wet steam supersonic nozzle. International Journal of Thermal Sciences. 2022 Jan 1;171:107207.
[49] Bakhtar F, Young JB, White AJ, Simpson DA. Classical nucleation theory and its application to condensing steam flow calculations. Proceedings of the Institution of Mechanical Engineers, Part C: Journal of Mechanical Engineering Science. 2005 Dec 1;219(12):1315-33.
[50] Petruccelli G, Grönman A, Turunen-Saaresti T. A Novel Numerical Approach for Simulating Low-Pressure and High-Pressure Non-Equilibrium Condensation in Real Gases. International Journal of Multiphase Flow. 2023 Dec 13:104700.
[51] Zhang G, Li Y, Jin Z, Dykas S, Cai X. A novel carbon dioxide capture technology (CCT) based on non-equilibrium condensation characteristics: Numerical modelling, nozzle design and structure optimization. Energy. 2024 Jan 1;286:129603.
[52] Aliabadi MA, Zhang G, Dykas S, Li H. Control of two-phase heat transfer and condensation loss in turbine blade cascade by injection water droplets. Applied Thermal Engineering. 2021 Mar 5;186:116541.
[53] Wróblewski W, Dykas S, Gardzilewicz A, Kolovratnik M. Numerical and experimental investigations of steam condensation in LP part of a large power turbine. Journal of fluids engineering. 2009;131(4).
[54] Zhang G, Wang X, Pourranjbar D, Dykas S, Li H, Chen J. The comprehensive analysis of the relationship between the latent heat, entrainment ratio, and ejector performance under different superheating degree conditions considering the non-equilibrium condensation. Applied Thermal Engineering. 2022 Jan 5;200:117701.

[55] Moses CA, Stein GD. On the growth of steam droplets formed in a Laval nozzle using both static pressure and light scattering measurements.
[56] Sun W, Ma X, Ma S, Zhang H, Zhang L, Xue H, Jia L. Effects of surface roughness and temperature on non-equilibrium condensation and entrainment performance in a desalination-oriented steam ejector. Applied Thermal Engineering. 2021 Sep 1;196:117264.
[57] Mazzelli F, Giacomelli F, Milazzo A. CFD modeling of condensing steam ejectors: Comparison with an experimental test-case. International Journal of Thermal Sciences. 2018;127:7-18.
[58] Suvarnakuta N, Pianthong K, Sriveerakul T, Seehanam W. Performance analysis of a two-stage ejector in an ejector refrigeration system using computational fluid dynamics. Engineering Applications of Computational Fluid Mechanics. 2020 Jan 1;14(1):669-82.
[59] Ruangtrakoon N, Thongtip T. An experimental investigation to determine the optimal heat source temperature for R141b ejector operation in refrigeration cycle. Applied Thermal Engineering. 2020 Apr 1;170:114841.
[60] Al-Doori G, Buttsworth DR. Pitot pressure measurements in a supersonic steam jet. Experimental Thermal and Fluid Science. 2014 Oct 1;58:56-61.

[65] Drucker H, Burges CJ, Kaufman L, Smola A, Vapnik V. Support vector regression machines. Advances in neural information processing systems. 1996;9.
[66] Suykens JA, Vandewalle J. Least squares support vector machine classifiers. Neural processing letters. 1999 Jun;9:293-300.
[67] Cherkassky V, Shao X, Mulier FM, Vapnik VN. Model complexity control for regression using VC generalization bounds. IEEE transactions on Neural Networks. 1999 Sep;10(5):1075-89.
[68] Smola AJ, Schölkopf B. A tutorial on support vector regression. Statistics and computing. 2004 Aug;14:199-222.
[69] de Melo VV, Banzhaf W. Drone Squadron Optimization: a novel self-adaptive algorithm for global numerical optimization. Neural Computing and Applications. 2018 Nov;30:3117-44.